Lawrence Berkeley National Laboratory

Lawrence Berkeley National Laboratory

Title

Nuclear fragmentation cross sections for NASA database development

Permalink

https://escholarship.org/uc/item/4ht9w05q

Authors

Zeitlin, Cary J.
Heilbronn, Lawrence H.
Miller, Jack
et al.

Publication Date

2001-08-24

eScholarship.org Powered by the California Digital Library
University of California

Nuclear Fragmentation Cross Sections for NASA Database Development

C. Zeitlin[1], L. Heilbronn[1], J. Miller[1], A. Fukumura[2], Y. Iwata[2], T. Murakami[2], J. MacGibbon[3], L. Pinsky[3], T. Wilson[4]

1. *Lawrence Berkeley National Laboratory, Berkeley, California 94720*
2. *National Institute of Radiological Sciences, Chiba, Japan*
3. *Physics Department, University of Houston, Houston, Texas, 77204*
4. *NASA Johnson Space Center, Houston, Texas 77058*

Abstract. Heavy ions with energies of hundreds to thousands of MeV/nucleon are present in the Galactic Cosmic Rays and will be a source of risk to astronaut health when long-duration crewed missions are undertaken. Nuclear interactions of these GCR ions in shielding materials must be accurately modeled by transport codes in order to estimate the dose and dose equivalent at points inside a spacecraft. Uncertainties in the nuclear fragmentation cross sections are propagated into these estimates, and the overall uncertainties increase as shielding depth increases. A program of fragmentation cross section measurements has therefore been undertaken to reduce these uncertainties, using GCR-like ion species and energies in particle accelerators in the United States, at the Brookhaven National Laboratory's Alternating Gradient Synchrotron (AGS) and in Japan at the National Institute of Radiological Science's Heavy Ion Medical Accelerator in Chiba (HIMAC). An extensive set of data has been obtained with beams ranging from helium to iron and including most of the species that are prominent in the GCR.

INTRODUCTION

The flux of heavy ions in the Galactic Cosmic Radiation has been measured [1] and modeled [2] accurately, including the substantial variations modulated by the 11-year solar cycle. Ions as heavy as iron are common, with broad energy distributions ranging from 100 MeV/nucleon to several GeV/nucleon and higher. Astronauts on long-duration missions outside the geomagnetosphere will be exposed to these ions, many of which have ranges far greater than the depth of any practical shielding. Although ions heavier than He comprise only 2% of the GCR flux, their contributions to dose will be much greater, since dose is related to deposited energy which goes as the square of the ion's charge Z. Shielding the interior of a spacecraft by stopping all incident ions is not possible, and even if it were practical to deploy walls with very high areal densities, incident ions would undergo fragmentation and secondaries (and higher-generation) fragments, including neutrons, would still reach the interior. In more likely scenarios, shielding will consist of a variety of materials, with depths of 5–10 g cm^{-2} distributed inhomogeneously throughout the spacecraft.

A recent NASA report [3] summarizes the situation with regard to GCR-induced cancer: "(B)ecause of their higher energies, the cancer risk from GCR cannot be eliminated using operational approaches and practical amounts of radiation shielding." Since eliminating the risk is not possible, it is necessary to mitigate the risk by careful choice of shielding materials. The accurate modeling of ion transport through shielding is an essential part of this program. This in turn requires accurate knowledge of fragmentation cross sections; large uncertainties in cross sections can lead to large uncertainties in the conclusions one draws regarding the efficacy of shielding [4]. Although the uncertainties in biological response to heavy-ion exposure are much larger than the uncertainties in fragmentation cross sections [3], it is nonetheless beneficial to improve the transport codes [5], which ultimately depend on experimental data. A collaborative effort on both experimental and theoretical fronts has been active for several years and includes groups from Lawrence Berkeley National Laboratory, the Japanese National Institute of Radiological Sciences, NASA Headquarters, NASA Langley Research Center, NASA Johnson Space Center, the University of Tennessee, and the University of Houston.

FRAGMENTATION EXPERIMENTS

Measurements Along the Beam Axis

Using a silicon detector stack and standard electronics [6], an extensive set of data has been obtained with the detectors placed directly downstream from targets of varying compositions and depths. A typical data set includes runs taken with at least five target materials – carbon, polyethylene, aluminum, copper, and lead. Cross sections on hydrogen can be extracted by subtracting carbon-target cross sections from those obtained with polyethylene targets. In most cases, we take runs with two or three different depths of each material; because the cross sections cannot depend on target depth, the redundant measurements allow us to study systematic errors in detail. Table 1 lists the beam ions and energies for which we presently have full data sets. In each measurement, silicon detectors of various sizes are placed at specific points downstream of the target so as to subtend particular acceptance angles, as depicted schematically in Fig. 1 for a typical HIMAC experiment. Plastic scintillators are used for pulse height and time-of-flight analysis, and the NaI crystal placed at the end of the beamline gives a total-energy measurement.

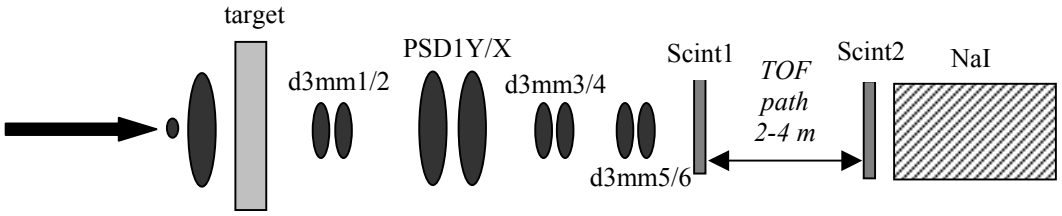

FIGURE 1. Schematic drawing of a typical beamline setup for an experiment at the HIMAC. Beam is incident from the left.

The beamline layout sketched above shows two silicon detectors upstream of the target, one quite small (50 mm^2 active area, 300 μm depth) and one much larger (either 3 mm thick with 450 mm^2 active area or 5 mm thick with 1400 mm^2 active area). These two detectors are used to trigger the readout of the electronics and, in the off-line data analysis, to identify events in which a single beam ion traversed both without interacting and entered the target. The detectors downstream of the target include six 3 mm thick units – hence the designation d3mm1, d3mm2, etc. – with 450 mm^2 active areas, and a pair of 1 mm thick position-sensitive detectors (PSD's), one oriented to measure the X coordinate and one to measure Y (the beam axis defines the Z coordinate). All the silicon detectors are lithium-drifted and are biased to full depletion; each detector gives a measurement of deposited energy ΔE. Fragments and primary ions that survive the target are identified in scatter-plots of, e.g., ΔE in d3mm2 vs. ΔE in d3mm1, as shown by the example in Fig. 2 (obtained with a 400 MeV/nucleon ^{28}Si beam incident on a 2.9 g cm^{-2} CH_2 target).

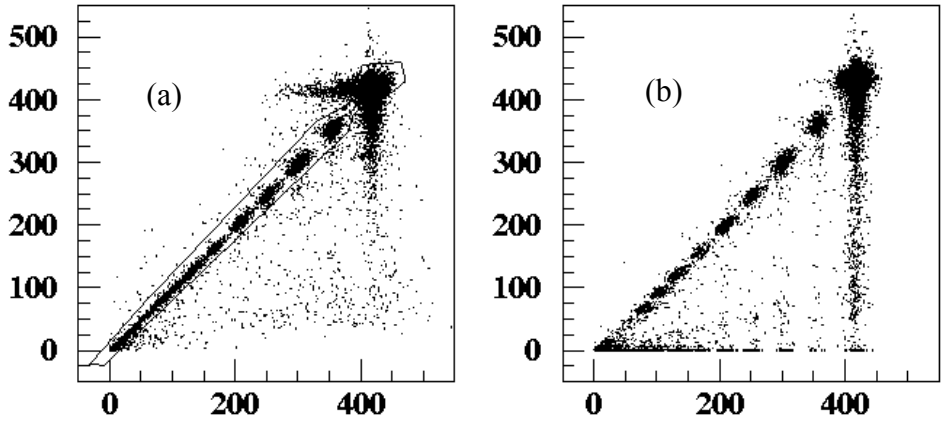

FIGURE 2. Scatter plots of ΔE correlations in (a) d3mm2 vs. d3mm1, (b) d3mm4 vs. d3mm1. Both are from the same data set, with a 400 MeV/nucleon ^{28}Si beam incident on a 2.8 g cm^{-2} CH_2 target. All ΔE's are in MeV.

TABLE 1. Data sets.

Beam Ions, E (MeV/u)	Accelerator	largest θ	2nd θ	3rd θ
^{12}C, 290 & 400	HIMAC	8°	4°	2.5°
^{12}C, ^{14}N, ^{16}O, 400	HIMAC	7°	2.5°	1.2°
^{20}Ne, ^{28}Si, 600	HIMAC	8°	4°	2.5°
^{28}Si, 400	HIMAC	7°	2.5°	1.2°
^{28}Si, 600 & 1000	AGS	8°	4°	2.5°
^{56}Fe, 400	HIMAC	5°	1.2°	
^{56}Fe, 600 & 1060	AGS	3.5°	1.1°	0.5°

Figure 2(a) shows ΔE in d3mm2 vs. ΔE in d3mm1, along with a cut contour used to define the sample of "good" events (only events with well-correlated ΔE's are kept). Distinct islands of events corresponding to the primary Si and heavy fragments (down to about F) are obvious. At the moderately large acceptance of d3mm1/2 in this experiment (2.5°), the multiplicity of light fragments is such that no clear islands of lower-Z fragments can be seen in this plot. In contrast, Fig. 2(b), with ΔE in d3mm4 plotted on the ordinate, shows clusters for many more fragment species. The region of the plot below the 45° line is populated by events in which d3mm4 recorded significantly lower ΔE than did d3mm1. There are two classes of events with this signature: (1) those in which a particle undergoes a nuclear interaction in one of the detectors, and (2) those in which a fragment has a sufficiently large production angle so that it is seen in d3mm1 but is outside the much smaller acceptance of d3mm4. The band of events with very small or zero ΔE in d3mm4 can be seen to increase in density as d3mm1 decreases, due to the larger production angles of lighter "leading" fragments, which causes many of them to miss d3mm4, which may record no hit or a hit only by even lighter fragments (e.g., a H or He fragment).

Detected Spectra and Particle Identification Ambiguities

Fig. 3 shows fragment spectra obtained at three different acceptances with 400 MeV/nucleon ^{14}N ions incident on a Cu target. The N peaks have been suppressed in these histograms; the effective Z detected is scaled according to the primary peak locations in the corresponding histograms of ΔE. The spectrum in Fig. 3(a) is typical of large-acceptance spectra in that fragment peaks can be seen down to about half the beam charge. At smaller acceptances, as in 3(b) and 3(c), distinct peaks emerge for all fragment species, for the same multiplicity-related reasons that more detail is seen in Fig. 2(b) than in 2(a). Peaks also appear for some particular combinations of fragments detected in coincidence. Multiple-fragment peaks in Fig. 3(b) and 3(c) can be seen near charge 4.4 (from events with a Be fragment in coincidence with a He fragment), and at Z ≈ 3.5 (from events with three He fragments detected). The detected Z goes as the square root of the sum of the fragment charges squared, so three-He events appear at Z = $\sqrt{12}$ = 3.46, as observed. This behavior also makes the "charge 3" peak ambiguous: with unsegmented detectors, one cannot distinguish events with a Li fragment (Z =3) from those in which two He fragments (effective Z = 2.8) are detected in coincidence. The finite widths of the fragment velocity distributions cause the ΔE distributions for the two types of events to overlap considerably. We have recently underaken a new approach to this problem by implementing a silicon strip detector (SSD) in the experiment. A scatterplot obtained with 400 MeV/nucleon ^{12}C is shown in Fig. 4, showing separation of the two distributions into distinct clusters of events.

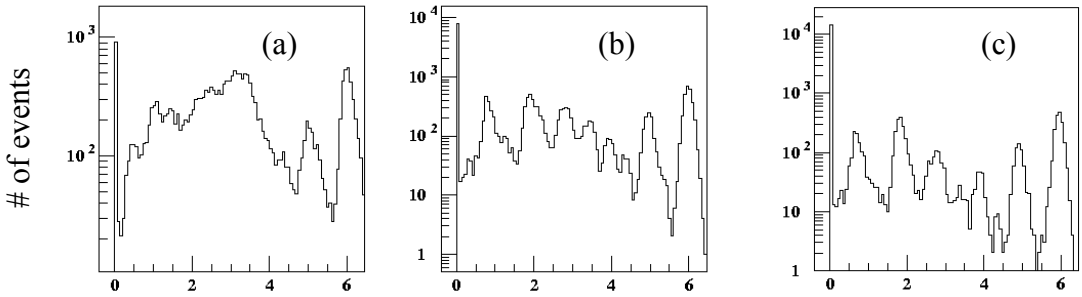

FIGURE 3. Histograms of detected Z at three different angular acceptances with a 400 MeV/nucleon ^{14}N beam incident on a Cu target with an areal density of 7.2 g cm^{-2}. The spectra were obtained with detectors at 7° (a), 2.5° (b), and 1.2° (c).

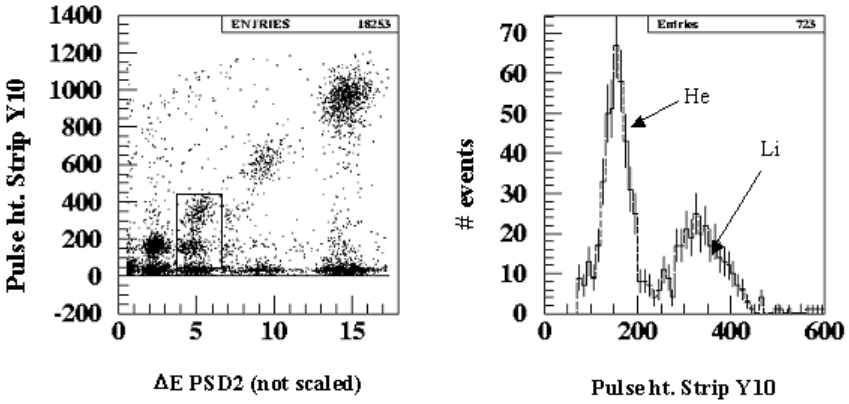

FIGURE 4. Left: scatter plot of ΔE in a single strip of the SSD vs. ΔE in an unsegmented PSD placed just downstream of the SSD for a 400 MeV/nucleon ^{12}C beam incident on a composite target. Events with a carbon ion are off-scale; the boxed region indicates the region populated by events with either a Li fragment or two He fragments. Using the PSD alone (i.e., taking a projection onto the x-axis) would yield a single peak of "ambiguous" events; taking a projection onto ΔE in the strip shows clear separation of the two event types.

In a recent article on the fragmentation of ^{20}Ne (7), a method for resolving some ambiguities in particle detection was described; the method makes use of the correlations between signals in the last silicon detector and the far-downstream plastic scintillator and does not depend on spatial segmentation of the detectors. It was shown that, at least for a Ne beam, a majority of apparent "charge 4" events seen in d3mm5/6 were due to the detection of four He fragments. In the same article, we described in detail the methods for extracting charge-changing and fragment production cross sections from histograms analogous to those in Fig. 3. The same methods are applicable to all the data sets discussed here. For fragment species with Z's near the beam charge, little fall-off was seen in the cross sections obtained at 7° compared to those obtained at 2.4°; this is because the fragment angular distributions are strongly forward-peaked when only a few nucleons are removed from the projectile, in keeping with the predictions of Goldhaber's statistical model of fragmentaton (8). As fragment charge and mass decrease, angular distributions broaden and significant decreases are seen in the cross sections obtained at small angles. The loss of fragments at small acceptance causes the number of events at Z = 0 (no charged fragment inside the detector acceptance) to increase, as can be seen clearly in the Fig. 3 histograms. The same effect is also observed in preliminary results obtained with all other beams.

Results:Charge-Changing and Fragment Production Cross Sections, Model Comparisons, Angular Distributions

The methods used to extract the cross sections have been described in detail (7). Several corrections to the raw counts are needed, and these grow in importance as target depth increases. The corrections contribute to the overall systematic errors, which are typically about 3% for charge-changing cross sections, about 5% for fragment production cross sections for $Z_{frag} > Z_{beam}/2$, and 10-20% for the lighter fragment species. The light-fragment cross sections have generally not been reported in earlier fragmentation work. An example showing preliminary data is given in Fig. 5 for 600 MeV/nucleon ^{28}Si on aluminum and carbon targets; the results are compared to the semi-empirical nuclear fragmentation code NUCFRG2 (9), which was found to give good agreement with measured cross sections for ^{56}Fe on a variety of targets (10). The model is not very accurate below charge 12, and does not reproduce the observed enhancement of even-Z fragments and the relative suppression of odd-Z fragments.

Part of the large systematic uncertainties for the light fragments is due to uncertainties in the modeling of fragment angular distributions. Our beamline simulation code (7) has a single free parameter, σ_0, which controls the widths of the Gaussians that describe (as a function of A_{frag}) the distributions. This parameter is not known *a priori* and the existing experimental data – which have been summarized by Tripathi and Townsend (11), leading to a parametrization for σ_0 – are sparse. The acceptance-angle dependence of the cross sections we obtain is an indirect measure of this parameter over a wide range of beam and target masses. To obtain more direct information about fragment angular distributions, a program of measurements with silicon detectors placed at specific angles off the beam axis (2.5°, 4°, 5.5°, 7.5°, and 10°) has also been begun, using 600 and 800 MeV/nucleon ^{28}Si beams and a 600 MeV/nucleon ^{20}Ne beam. These data will yield $d\sigma/d\theta$ at specific values of θ; fitting these results to Gaussian distributions will determine the appropriate values of σ_0 and allow us to make a direct test of the angular

distributions predicted by the parametrization of Ref. (11). It will also be possible to see deviations from Gaussian shapes, as expected for the lightest fragments.

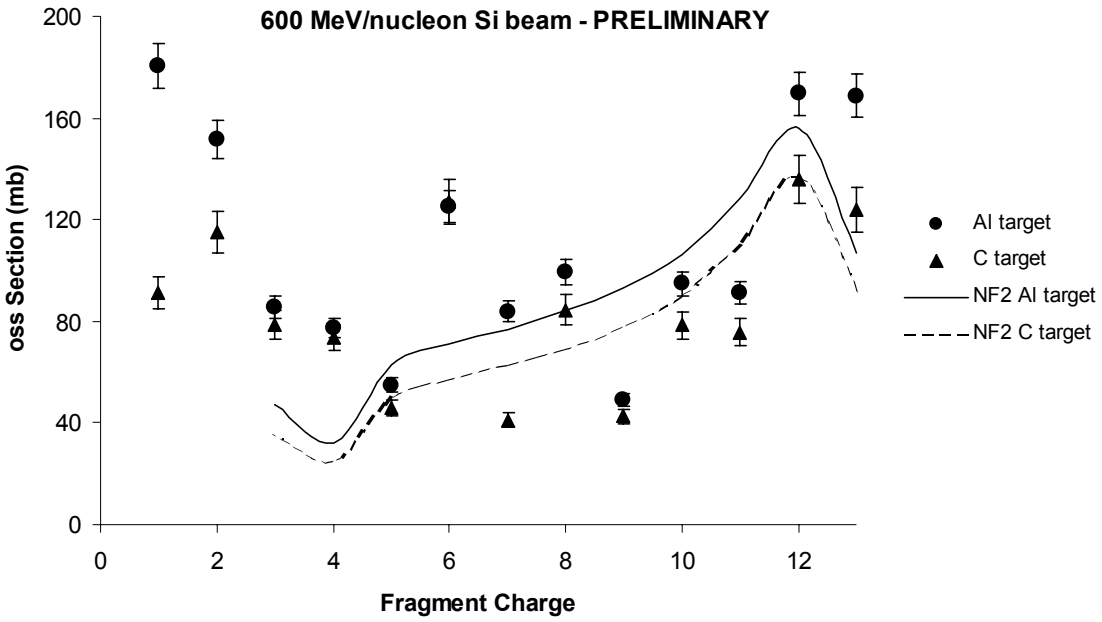

FIGURE 5. Preliminary fragment production cross sections for 600 MeV/nucleon silicon on carbon and aluminum targets, compared to the predictions of the NASA Langley model code NUCFRG2 (abbreviated to NF2 in the figure legend).

ACKNOWLEDGMENTS

This work was supported at LBNL by the Space Radiation Health Program of the National Aeronautics and Space Administration under NASA Grant Numbers L14230C and H31909D, through the U.S. Department of Energy under Contract No. DE-AC03076SF00098. At HIMAC, this work was supported in part by the Research Project with Heavy Ions at NIRS-HIMAC, Project Number 9P037. At the University of Houston, this work was supported by NASA Grant No. NAG8-1658.

REFERENCES

1. J. A. Simpson, in Composition and Origin of Cosmic Rays, edited by M. M. Shapiro (Reidel, Dordrect, 1983), p. 1
2. A. J. Tylka, J. H. Adams, Jr., P. R. Boberg, B. Brownstein, W. F. Dietrich, E. O. Flueckiger, E. L. Petersen, M. A. Shea, D. F. Smart, and E. C. Smith, IEEE Trans. Nucl. Sci. 44, 2150-2160 (1997).
3. F. A. Cucinotta, W. Schimmerling, J. W. Wilson, L. E. Peterson, G. D. Badhwar, P. B. Saganti, and J. F. DiCello, NASA JSC Internal Report JSC-29295 (2001), on the Internet at http://srhp.jsc.nasa.gov/Newsletter/Volume1-2/MarsRisk.pdf
4. J. W. Wilson, M. Kim, W, Schimmerling, F. F. Badavi, S. A. Thibeault, F. A. Cucinotta, J. L. Shinn, and R. Kiefer, Health Phys. 68, 50 (1995).
5. J. L. Shinn, J. W. Wilson, F. F. Badavi, E. V. Benton, I. Csige, A. L. Frank, and E. R. Benton, Radiat. Meas. 23, pp. 57-64 (1994).
6. C. Zeitlin et al., Radiat. Meas. 23, pp. 65-81 (1994).
7. C. Zeitlin et al., Phys. Rev. C 64, 024902 (2001).
8. A. S. Goldhaber, Phys. Lett. 53B, 306 (1974).
9. J. W. Wilson, J. L. Shinn, L. W. Townsend, R. K. Tripathi, F. F. Badavi, and S. Y. Chun, Nucl. Instr. Meth. B 94, 95 (1994).
10. C. Zeitlin et al., Phys. Rev. C 56, pp. 388-397 (1997).
11. R. K. Tripathi and L. W. Townsend, Phys. Rev. C 49, pp. 2237-2239 (1994).